ORIGINAL RESEARCH

Facile and mild method to fabricate a flexible cellulose-based electrode with reduced graphene and amorphous cobalt–iron–boron alloy for wearable electronics

Wei Wang · Tao Li · Yinyin Sun · Leigen Liu · Jianbing Wu · Gang Yang · Baojiang Liu

Abstract Developing a novel flexible textile-based electrode with splendid electrochemical performance for seamless embedding in smart clothing remains a huge challenge. In this work, amorphous Co–Fe–B alloy@RGO@cotton fabric flexible electrode with outstanding electrochemical properties was prepared through dipping-drying method and chemical reduction method at room temperature. The electrochemical performance of this resultant composite material could be controlled by adjusting the Co/Fe molar ratio. With the molar ratio of Co/Fe 2:1, this flexible electrode demonstrated the maximum specific capacitance 302.6 F/g at the scan rate 5 mV/s. Even after 3000 cycles of charge and discharge or being folded for 300 times, the fabric flexible electrode also maintained the high specific capacitance retention, showing its superior stability and flexibility. In brief, this flexible Co–Fe–B@RGO@cotton fabric electrode with easy fabrication, low-cost, and splendid electrochemical performance offers promising prospects in the field of flexible and wearable electronics.

Keywords Amorphous · Fabric flexible electrode · Co–Fe–B@RGO@fabric

W. Wang · T. Li · Y. Sun · L. Liu · J. Wu
Department of Textitle &Garment Engineering, Changshu Institute of Technology, Suzhou 215500, China

W. Wang · G. Yang (✉)
Jiangsu Laboratory of Advanced Functional Materials, Department of Chemistry, Changshu Institute of Technology, Suzhou 215500, China
e-mail: gyang@cslg.edu.cn

B. Liu (✉)
College of Chemistry, Chemical Engineering & Biotechnology, Donghua University, Shanghai 201620, China
e-mail: bjliu@dhu.edu.cn

Introduction

Flexible wearable electronic equipment is developing rapidly because its use has brought about great changes to people's lives like the application of Google Glass, implantable medical devices and so on (Allison et al. 2017; Li et al. 2019a, b; Tebyetekerwa et al. 2019). As an important and indispensable part, flexible and lightweight energy storage devices with outstanding electrochemical performance must be developed to meet the growing requirements of these personalized electronic technologies (Li et al. 2019a, b; Shen et al. 2017). Thereinto, supercapacitor is considered as one of the most promising power storage system due to its appealing properties like ultrahigh power delivery and excellent life cycle (Heo et al. 2018; Liu et al. 2018; Sung et al. 2018). Also developing suitable flexible substrates and novel electrode active materials with high electrochemical performance are two critical factors to design and prepare flexible supercapacitor.

Numerous flexible and lightweight substrates involved paper (Dong et al. 2016; Lin et al. 2017), film (Chen et al. 2018; Hu et al. 2018; Luo et al. 2018; Nystrom et al. 2015; Zhang et al. 2015), spong (Akanksha et al. 2019; Kyu et al. 2017), textile (Lima et al. 2018), carbon fabric (Sun et al. 2019; Wang et al. 2019a, b) and other flexible materials (Liang et al. 2018; Qiu et al.2015; Wang et al. 2014a, b) were extensively studied to prepare the flexible electrode. Textile fabrics have been regarded as the ideal candidate for the flexible electrode on account of their porous nature, three-dimensional (3D) structure, large surface area and desirable mechanical property (Jeong et al. 2019; Liu et al. 2018). Moreover, textile-based capacitors could be seamlessly integrated with clothing and garment. However, the fabric is the typical non-conductor with the specific resistance of 10^6–10^7 Ω/sq (Zhao et al. 2017). Therefore, it is indispensable to endow traditional fabric with high conductivity to obtain high performance electrode.

Carbon materials involving carbon nanotube (Li et al. 2019a, b), activated carbon (Xu et al. 2017) and graphene (Chee et al. 2016; Feng et al. 2018) are one kind of the most applied active materials in the fabrication of textile-based supercapacitor. This use not only attributed to their good electrical conductivity, but also their double layer capacitance properties. Among these carbon materials, graphene is deemed to a splendid conductive material and double layer capacitor material for energy storage devices because of its salient features, such as large specific surface area, stable chemical properties and corrosion resistance (Li et al. 2019a, b; Wang et al.2014a, b; Xing et al. 2019). The large amount of hydroxyl and carboxyl on the structure of graphene is conducive to depositing it on the surface of the fabric surface (Kowalczyk et al. 2017). Therefore, research on graphene/textile composite electrode is growing rapidly, and lots of devices with high performance have been reported. Graphene/cotton fabric electrode with specific capacitance of 40 F/g was prepared via dipping-drying method in Xu's report (Xu et al. 2015a, b). Xing's research team also prepared RGO-coated fabric with high potential window and excellent cycling stability through dry-coating method, followed by chemical and microwave reduction (Li et al. 2019a, b). However, the lower energy density of graphene/cotton cannot meet the requirements for

wearable electronic system resulting from energy storage mechanism of dual-layer materials.

To fabricate high performance electrode, pseudocapacitive active substances like transition metal compound or conductive polymer are widely used to combine with carbon materials because of their high energy densities (Chen et al. 2017; Xiang et al. 2017). Among them, transition metal compound materials contained metal oxides, metal hydroxides, metal sulphides and metal selenides, have been demonstrated to display outstanding electrochemical property (Senthilkumar et al. 2016; Wen et al. 2016; Yang et al. 2014). Recently, the application of transition metal boride (boron alloy) also has been extended to wearable electronics from the field of electrocatalysis, luminescence, oxygen evolution reaction and thermoelectric (Raula et al. 2012; Wang et al. 2019a, b; 2015, Zhou et al. 2012). Transition metal borides like Ni-Co-B, Ni–B and Co–Fe–B have been confirmed to exhibit super electrochemical performance accompanied by the efficient ion and electron transport ability (Li et al. 2018a, b; Meng et al. 2019; Qin et al. 2018). Set current density as 1 A/g, the specific capacitance of amorphous Co–Fe–B alloy could reach 981F/g, showing prominent electrochemical performance (Meng et al. 2019). The specific capacity of Ni–B alloy was up to 137.9 mAh/g, which was ascribed to large surface area and inherent abundant defects. Notably, these metal borides were all amorphous materials with long-range disordered and short-range ordered property (Qin et al. 2018). According to previous literature (Li et al. 2018a, b; Sayyed et al. 2017), larger surface area, more grain boundaries and ion diffusion channels of amorphous materials are beneficial for improving the electrochemical performance (Li et al. 2018a, b). However, up to date, only these reports focused on the energy storage properties of amorphous boron alloy. With these remarkable electrical conductivity, outstanding electrochemical reactivity, easy to process and low-cost nature, amorphous transition metal borides should be paid more effort to further expand their application and develop their charging and discharging mechanism.

In this paper, Co–Fe–B amorphous material attached on RGO coated textile was firstly fabricated by a facile dipping-drying method, followed with chemical reduction technology. The preparation conditions are simple and mild, avoiding the damage of heat treatment to mechanical properties of textile

fabric. The morphologies and electrochemical performances of as-made electrodes with different Co/Fe ratios were systematically investigated. The optimum electrode exhibited high specific capacitance and good cycle stability. This novel amorphous ternary Co–Fe–B alloy@RGO@textile electrode is a promising candidate for cost-effective practical application in the field of wearable electronic.

Experimental procedure

Materials

Sodium hydroxide (NaOH), sodium borohydride ($NaBH_4$), sodium sulfate (Na_2SO_4), cobalt nitrate hexahydrate ($Co(NO_3)_2 \cdot 6H_2O$) and ferric chloride hexahydrate ($FeCl_3 \cdot 6H_2O$) were obtained from Sinopharm Chemical Reagent Co., Ltd. All reagents were of AR grade without any further processing. Graphene oxide (GO) was purchased from Beijing Boyu Co., Ltd. Woven cotton fabric was purchased from Shaoxing Aobang Textile Company.

Preparation of RGO@cotton fabric composite

RGO@cotton fabric composite electrode was prepared using dipping-drying method according to previous report (Xu et al. 2015a, b). 1 g of GO powders were added into 0.5L of double-distilled water under stirring. The above suspension was sonicated for 30 min. And the commercial cotton fabric was rinsed using NaOH aqueous solution (1 mol/L) at 100 °C for 1 h. After being washed and dried, the treated fabric was immersed into GO dispersion for 30 min at normal temperature, and then dried at 60 °C for 2 h. This dipping-drying process was repeated for ten times to increase the load amount of GO. Finally, 0.6 mol/L of $NaBH_4$ was used as reductant to prepare RGO@cotton fabric composite.

Preparation of amorphous Co–Fe–B alloy@RGO@cotton fabric electrodes

The preparation method of Co–Fe–B @RGO@cotton fabric electrode was modified based on Meng's report (Meng et al. 2019). Detailed process was as followed:

$Co(NO_3)_2 \cdot 6H_2O$ powders and $FeCl_3 \cdot 6H_2O$ powders were dissolved in 100 mL deionized water to form clear solution A. 5 mmol NaOH and 25 mmol $NaBH_4$ were added into 50 mL deionized water to form solution B. Then, RGO@cotton fabric with size of 1*2 cm^2 was immersed into solution A for 30 min. Therewith, solution B was slowly added into solution A drop by drop. The resulting solution was magnetically stirred for another 10 min. Finally, Co–Fe–B @RGO@cotton fabric electrode was washed with double-distilled water and ethanol to eliminate possible impurities thoroughly, then dried at 60 °C for 12 h. The total molar of Co^{2+} and Fe^{3+} was 6 mmol. The molar ratio of Co/Fe was set as 1:2, 1:1, 2:1, and 3:1, corresponded to as-made sample Co1-Fe2-B@RGO@coton fabric, Co1–Fe1–B@RGO@cotton fabric, Co2–Fe1–B@RGO@cotton fabric, and Co3–Fe1–B@RGO@cotton fabric, respectively.

Characterization

The surface sheet conductivity of fabric electrode was measured using four-point probe tester (RTS-8). The surface morphology of textile electrode was measured on the scanning electron microscopy (SEM, SU8010, Hitachi) and a JEM-2100 transmission electron microscope (TEM). The elemental distribution of as-prepared sample was analyzed via elemental mapping and energy dispersive spectrometer (SEM–EDS). Selected area electron diffraction (SAED) pattern was obtained from HR-TEM measurement. The crystal structure of textile electrode was detected by using an X-ray diffractometer (XRD) with Cu Kα (40KV, 200 mA) wavelength. X-ray photoelectron spectrometry (XPS, Thermo Scientific Escalab, USA) measurement was adopted to detect element compositions and chemical bonding states of textile electrode. The three-electrodes configuration (CHI660E Instruments) was used to measure cyclic voltammogram curves (CV) and galvanostatic charge/discharge curve (GCD) of fabric electrode in 1 mol/L Na_2SO_4 electrolyte with Ag/AgCl electrode, Pt foil and fabric electrode as reference electrode, counter electrode and working electrode, respectively. Electrochemical impedance spectra (EIS) was recorded in the frequency range from 100 kHz to 0.1 Hz.
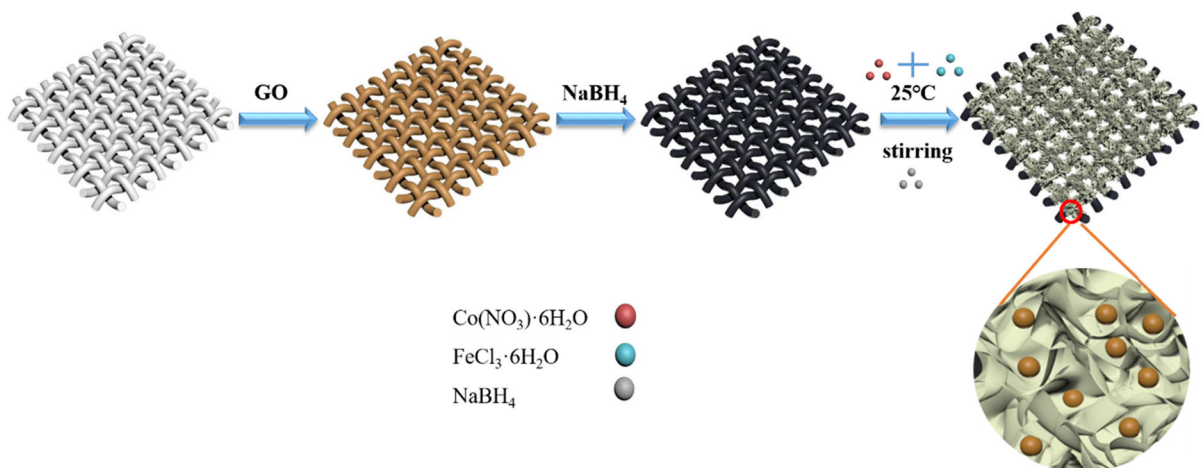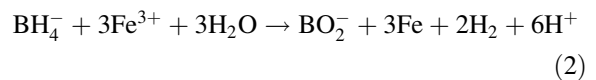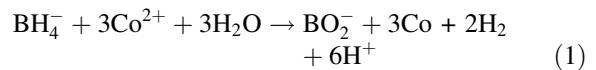
Results and discussion

Structure of amorphous Co–Fe–B alloy@RGO@cotton fabric electrode

Schematic diagram to prepare amorphous Co–Fe–B alloy@RGO@cotton fabric is shown in Fig. 1. As the conductive agent and double layer energy storage material, RGO nanosheets were uniformly deposited on the surface of cotton fabric substrate using dipping-drying method. Then, amorphous Co–Fe–B alloy evenly distributed onto the surface of RGO@cotton fabric through a facile chemical reduction method. The whole preparation process was carried out at room temperature, greatly reducing the damage to the mechanical properties of fabrics.

The morphologies and structures of textile electrodes with different Co/Fe molar ratio were measured with a scanning electron microscope, and results are shown in Fig. 2. Clearly, RGO sheet with a size of several micrometers coated on the fabric was of a wavy and wrinkled structure due to the deformation upon the exfoliation and restacking process from Fig. 2. After being introduced Co1-Fe2-B alloy, large sheet structure appears to be stripped into smaller pieces with a few nanometer on the fabric substrate, as shown in Fig. 3a, b and c. Changing Co/Fe molar ratio from 1:2 to 1:1, the nanosheet structure transformed into nanospheres with average diameters of 50–80 nm (Fig. 3d, e and f). Interestingly, these two kinds of morphologies included nanosheets and nanospheres were both detected in the as-made fabric electrode

with the Co/Fe molar ratio 2:1. As indicated in Fig. 3g, h and i, some nanospheres filled in the gaps between the nanosheets, which were favorable for exposing to electrolyte and shortening the distance of ion diffusion transportation. As for Co3–Fe1–B@RGO@fabric electrode, many nanospheres were wrapped by nanosheets, as shown in Fig. 3j, k and l. Co3–Fe1–B@RGO@fabric electrode was of flocculent-like structure. This result showed that the content ratio of cobalt and iron played an important role in the forming of this material structure. With the increase of cobalt content, the single structure of the material becomes an obvious graded structure.
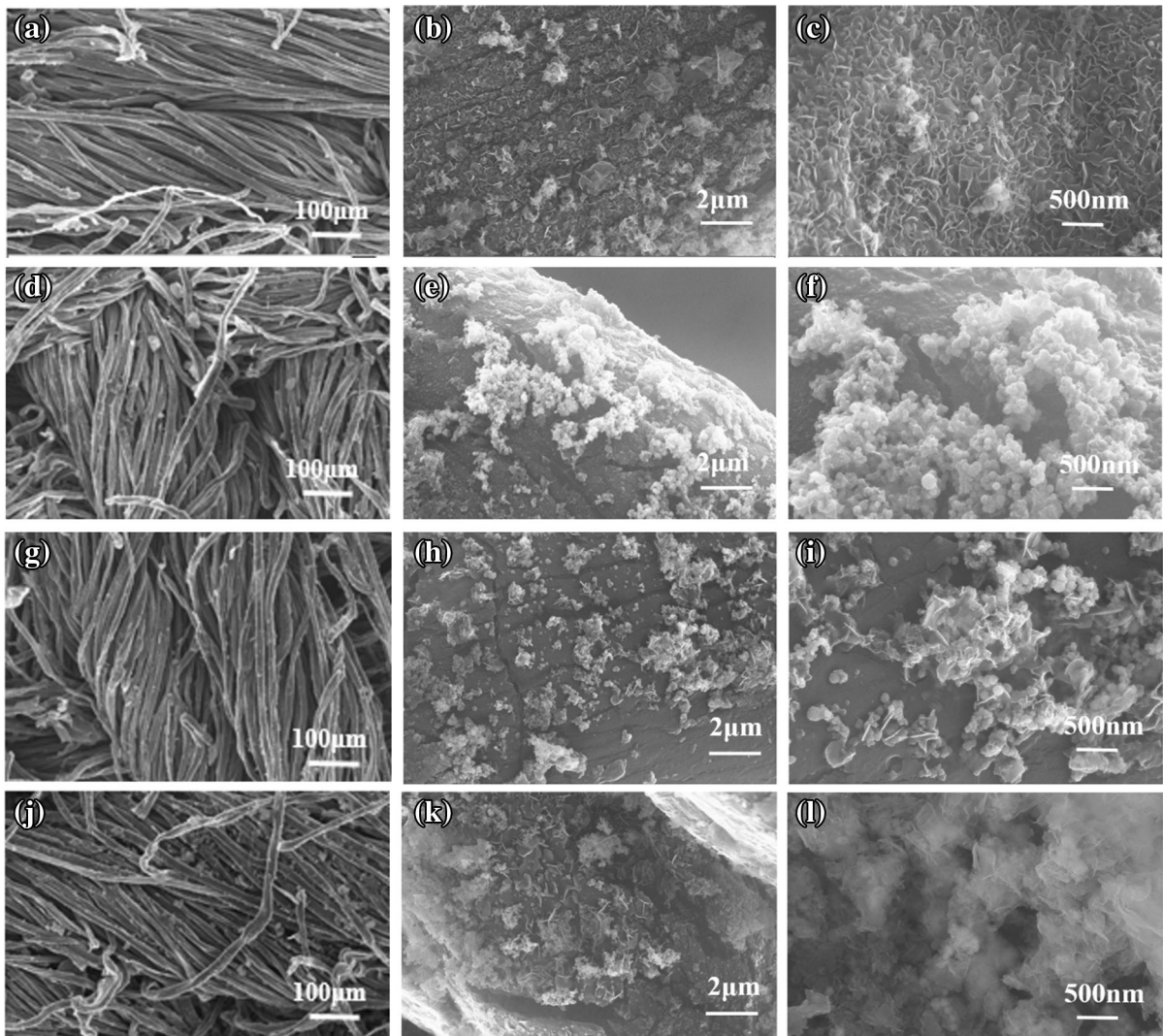
XRD patterns of textile electrodes with different Co/Fe molar ratio and original fabric are shown in Fig. 4. Obviously, the diffraction peaks at $2\theta = 14.36°, 16.36°, 22.60°$ and $33.98°$ were indexed as cellulose I of cotton fabric. As for textile electrodes with different Co/Fe molar ratio, no significant diffraction peaks of amorphous Co–Fe–B alloy and RGO were detected due to much weaker diffraction peaks compared with those of fabric substrate. The forming mechanism of Co–Fe–B was based on the following reactions (Sayyed et al. 2017; Wei et al. 2018).
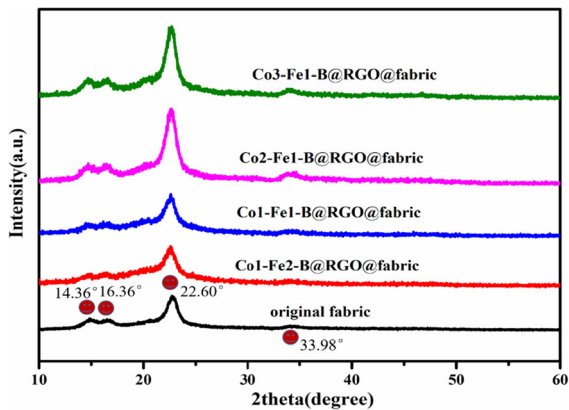
$$BH_4^- + 3Co^{2+} + 3H_2O \rightarrow BO_2^- + 3Co + 2H_2 + 6H^+ \quad (1)$$

$$BH_4^- + 3Fe^{3+} + 3H_2O \rightarrow BO_2^- + 3Fe + 2H_2 + 6H^+ \quad (2)$$

Fig. 1 Schematic synthesis of amorphous Co–Fe–B alloy@RGO@fabric electrode
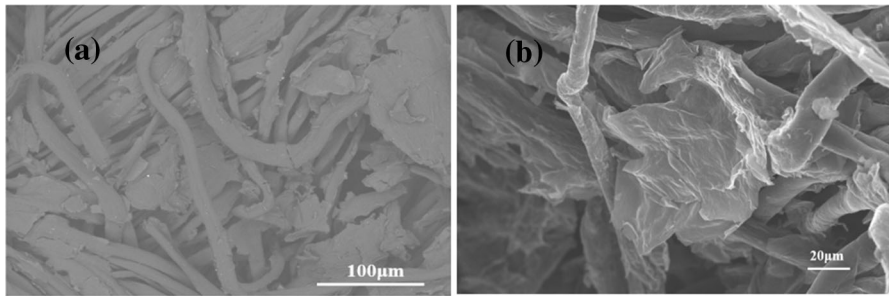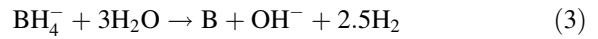
Fig. 2 SEM images of RGO@fabric material

**Fig. 3** SEM images with different magnification: Co1-Fe2-B@RGO@cotton fabric (**a**, **b**, **c**); Co1–Fe1–B@RGO@cotton fabric (**d**, **e**, **f**); Co2–Fe1–B@RGO@cotton fabric (**g**, **h**, **i**); and Co3–Fe1–B@RGO@cotton fabric (**j**, **k**, **l**)

Fig. 4 XRD patterns of original fabric and fabric electrodes with different Co/Fe molar ratio

$$BH_4^- + 3H_2O \rightarrow B + OH^- + 2.5H_2 \qquad (3)$$

Furthermore, EDS patterns of these fabric electrodes with different Co/Fe molar ratio were also conducted to verify the existence of Co–Fe–B, and the results are shown in Fig. 5a–d. Evidently, Fe, Co and B signals were originated from Co–Fe–B alloy. C and O peaks were ascribed to RGO and cotton fabric. The molar ratio of Co/Fe for different samples almost corresponded well to the proportion in the precursor mixture. For example, the molar ratio of Co/Fe of Co2–Fe1–B@RGO@fabric sample was close to 2:1 of the feed ratio. In addition, the elemental mapping analysis was also performed to characterize the distribution of these elements on the electrode surface, and the corresponding pictures are shown in Fig. 5e.
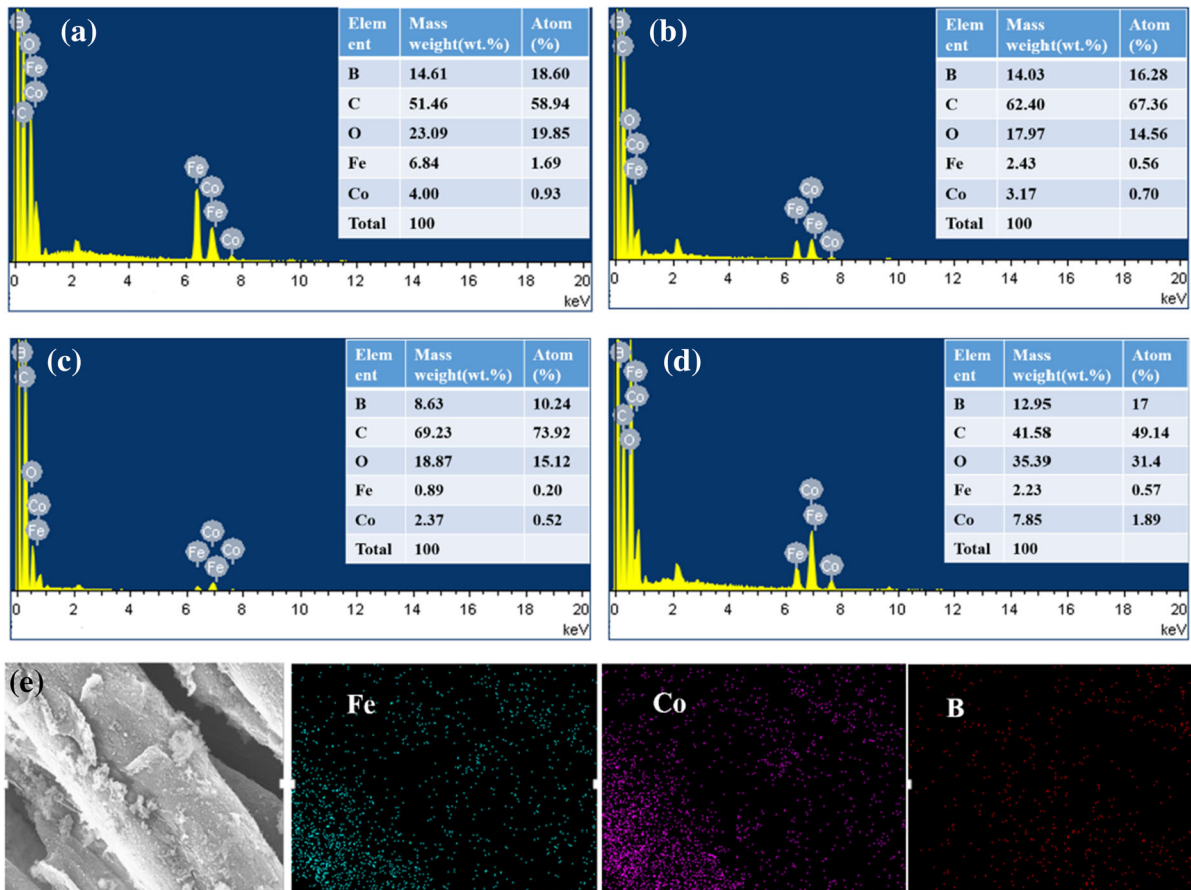

Fig. 5 EDS results of the as-made samples **a** Co1-Fe2-B@RGO@fabric; **b** Co1–Fe1–B@RGO@fabric; **c** Co2–Fe1–B@RGO@fabric; **d** Co3–Fe1–B@RGO@fabric; **e** elemental mapping of Co2–Fe1–B@RGO@fabric sample

The elements of Co, Fe and B were uniformly distributed on the surface of RGO@fabric composite, suggesting that Co–Fe–B alloy was successfully attached on the RGO@fabric surface, which was consistent with the above SEM results.

The surface element composition and element valence of this Co2–Fe1–B@RGO@fabric electrode were determined using XPS technology. All binding energies obtained were calibrated according to C 1 s peak from graphitic carbon at 284.55 eV. The full survey spectrum of Co2–Fe1–B alloy@RGO@fabric composite was shown in Fig. 6a. The high-resolution XPS spectral signals of different element are shown in Fig. 6b–f. As indicated in Fig. 6b, four peaks at
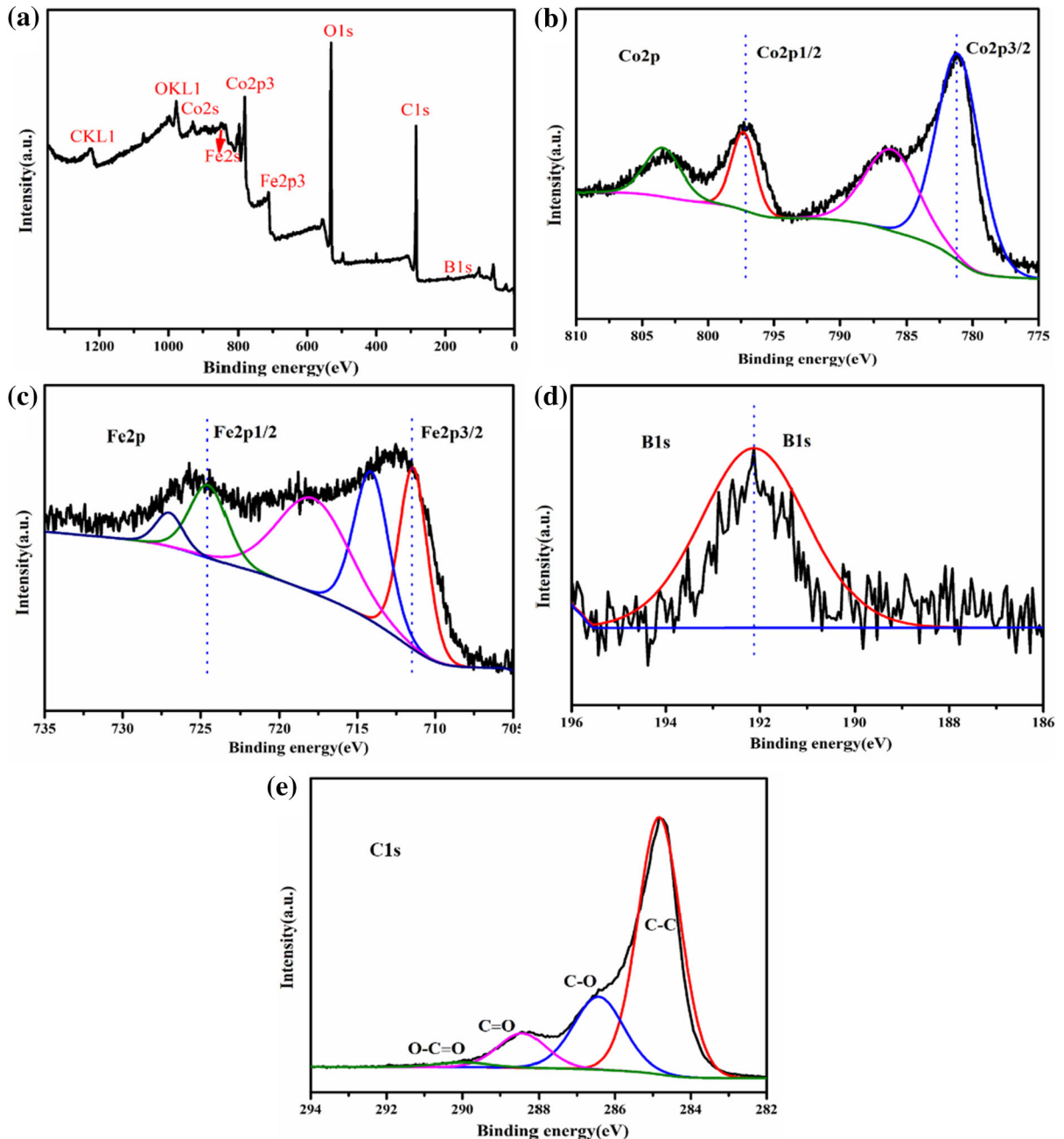
Fig. 6 XPS spectra of as-made sample with Co/Fe of 2:1 **a** full scan spectra; **b** Co 2p; **c** Fe 2p; **d** B 1 s; **e** C 1 s

781.2 eV, 786 eV, 796.74 eV and 803.45 eV are observed in the Co2p spectrum of Co2–Fe1–B@RGO@fabric composite. The peaks at 796.74 eV and 781.2 eV were attributable to Co2p1/2 and Co2p3/2 in the Co 2p spectrum. Peaks at 786 eV and 803.45 eV were assigned to shake-up satellite peaks. This result showed that cobalt existed in elemental and oxidation states. In Fig. 6c, XPS peaks of Fe 2p centered at 711.8 eV and 725.7 eV were assigned to Fe 2p3/2 and Fe 2p1/2, respectively. In addition, other three weak peaks of 713.9 eV, 718.3 eV and 730.6 eV were characterized as satellite peaks of Fe2p spectrum, suggesting the presence of both elemental and oxidized states. The B1s spectrum of Co2–Fe1–B alloy@RGO@fabric composite displayed one peak at 192.17 eV, which showed that boron was in oxidized states (Sayyed et al. 2017). In the high-resolution XPS spectra of C1s (Fig. 6e), four peaks at 289.2 eV, 288.3 eV, 286.5 eV and 285.6 eV were in agreement with O-C = O, C = O, C-O and C–C, respectively. The peaks of C = O and O-C = O reflected the existence of RGO (Xiang et al. 2017). Based on the above results, Co–Fe–B and RGO were confirmed to coexist in the Co2–Fe1–B@RGO@fabric electrode composite.

Figure 7 depicts TEM images for the structure and composition units of Co2–Fe1–B@RGO composite on the surface of fabric. Before TEM measurement,

the Co2–Fe1–B@RGO@fabric electrode was treated with ultrasound for 1 h to make Co2–Fe1–B and RGO drop from off the cotton fabric. From Fig. 7a–c, Co–Fe–B alloy was well anchored on the surface of RGO. It also proved that this product consisted of loose flower-like morphology. From HR-TEM image in Fig. 7c, no obvious crystal lattice can be detected. This result showed that Co2–Fe1–B alloy was of the amorphous structure. Also, SAED image in Fig. 7d clearly presented the broad and diffused halo ring which verified the amorphous nature of Co2–Fe1–B alloy rather than well-defined single crystal. These conclusions were consistent with the results observed from SEM. According to previous reports, the essential defects or vacancies and long-range atomic arrangement disorder of the amorphous materials were beneficial for their excellent electrochemical performance (Li et al. 2018a, b; Meng et al. 2019).

Electrochemical property of amorphous Co–Fe–B alloy@RGO@cotton fabric electrode

The effect of Co/Fe molar ratios on the electrochemical performances of as-made fabric electrodes were analyzed with a three-electrode configuration, and the result is shown in Fig. 8a. CV curves of these fabric electrodes exhibited the approximately symmetric and rectangular shape, showing the good capacitor
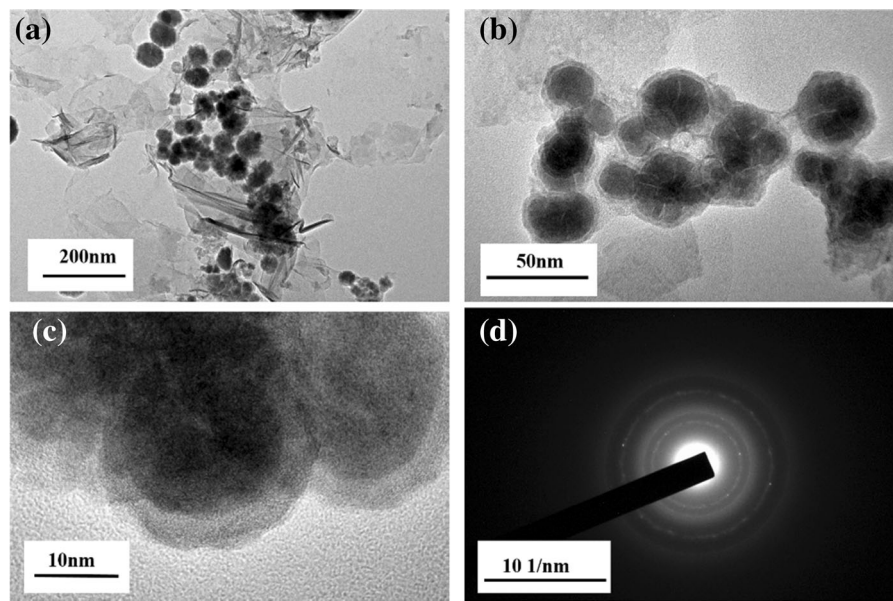
Fig. 7 TEM images of Co2–Fe1–B@RGO@fabric. **a**, **b** TEM images, **c** HRTEM Image, **d** SAED pattern
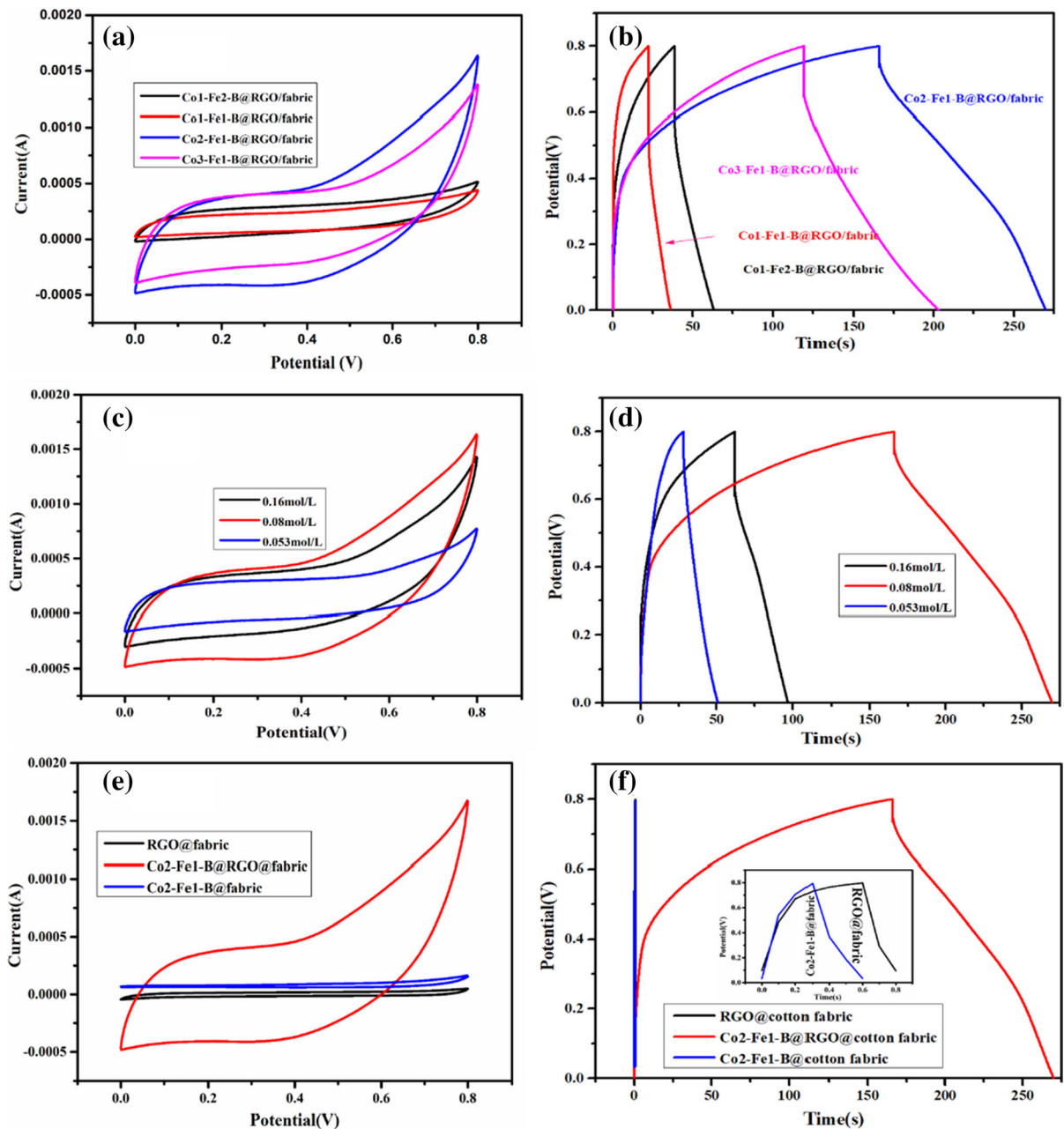
Fig. 8 a CV and **b** GCD curves of as-made samples with different Co/Fe molar; **c** CV and **d** GCD curves of Co2-Fe1-B@RGO@fabric samples with different raw reactant concentration; **e** CV and **f** GCD curves of RGO@fabric, Co2–Fe1–B@RGO@fabric, and Co2–Fe1–B@fabric electrodes

characteristic. Increasing the molar ratio of Co/Fe, specific capacitance first increased and then decreased. CV area of Co2–Fe1–B@RGO@fabric electrode was the largest among these four fabric electrode, indicating the best specific capacitance. Charge–discharge curves of these four fabric electrodes at the same

current density (0.5 mA/cm^2) are depicted in Fig. 8b. It was clear that Co2–Fe1–B@RGO@fabric electrode was of the longest charge–discharge time, showing it was of the best capacitive behavior. Maybe that the spherical and lamellar mixed structure of Co2–Fe1–B@RGO@fabric electrode were favorable for

exposing to electrolyte and shortening the distance of ion diffusion transportation.

To investigate the effect of the concentration of raw reactant on the electrochemical performance, CV and GCD curves of Co2–Fe1–B@RGO@fabric electrode with different concentration were compared, (10 mV/s; Fig. 8c and d). Obviously, Co2–Fe1–B@RGO@-fabric electrode with the concentration of 0.08 mol/L had the maximum integral CV area and the longest charge–discharge time, indicating the optimum electrochemical performance. Based on these results mentioned above, we deduced that the fabric electrode with the Co/Fe ratio 2:1 and the raw reactant concentration of 0.08 mol/L exhibited the best capacitive behavior.

Cyclic voltammogram curves of RGO@fabric electrode, Co2–Fe1–B@RGO@fabric electrode and Co2–Fe1–B@fabric electrode at the same scan rate of 10 mV/s were also measured to clarify the effect of electrode structure on electrochemical characters. As shown in Fig. 8e and f, CV curve area of Co2–Fe1–B@RGO@fabric electrode was the largest among these three electrode, and this electrode also exhibited a longer discharge time than Co2–Fe1–B@fabric electrode and RGO@fabric electrode. The low capacity of RGO@fabric electrode was ascribed to the double-layer mechanism. Although the specific capacitance of amorphous Co–Fe–B alloy was high (Meng et al. 2019), the cotton fabric is an insulator which resulted in a low electrochemical performance. Therefore, the combination of graphene sheets and amorphous Co2–Fe1–B created a synergistic effect to enhance the electrochemical capacitance. Generally, conductivity, crystalline structure and morphology of electrodes play the key effect on their electrochemical performance. The best electrochemical performance of Co2–Fe1–B@RGO@fabric was ascribed to its loose hierarchy nanostructure, which provide a high-speed pathway for ionic transportation to enhance electrochemical reaction. In addition, the incorporation of RGO could significantly improve electrical conductivity of composite electrode (as shown in Table 1), thus facilitating the transport of charge carriers. Moreover, amorphous Co–Fe–B alloy also had been confirmed to exhibit the good conductivity in previous report (Meng et al. 2019). Therefore, the synergistic effect of Co–Fe–B and RGO is beneficial for the high conductivity of Co2–Fe1–B@RGO@fabric.

In addition, CV curves of Co2–Fe1–B@RGO@-fabric composite material at variable scan rates from 5 mV/s to 50 mV/s are shown in Fig. 9a. All these curves were of nearly rectangular shape, indicating the outstanding electrochemical capacitor behavior even at higher scan rate of 50 mV/s. The specific capacitances were calculated from the CV curves were approximately 302.6F/g, 196F/g, 141F/g and 77.2F/g, corresponding to scan rate 5 mV/s, 10 mV/s, 20 mV/s and 50 mV/s, respectively (Fig. 9b). As expected, the specific capacitance decreased as the scan rate increased. Figure 9c showed the GCD curves of Co2–Fe1–B@RGO@fabric electrode under different current density. The composite electrode presented nearly similar curve shapes at current densities of 0.25 mA/cm^2, 0.5 mA/cm^2 and 1 mA/cm^2, demonstrating an ideal capacitor behaviour. To further study energy storage mechanism of Co2–Fe1–B@RGO@-fabric electrode, EIS measurement was studied. From the inset of Fig. 9d, the simulation circuit was fitted according to EIS spectra with Zview software. According to the previous reports (Allison et al. 2017; Li et al. 2019a, b, 2018a), Rs, Rct, CPE and Zw are four important parameters to analyze the ion transport ability of as-made electrode. Rs is the intercept of compressed arc at real axis, meaning the solution resistance resulted from the electrolyte. Rct is the diameter of the semiarc, depicting the charge transfer resistance arising from the interface between electrode and electrolyte, CPE is the constant phase unit and Zw is the Warburg diffusion resistance (Wan et al. 2017; Xu et al. 2015a, b). As for Co2–Fe1–B@RGO@fabric, Rs value is 20.02 Ω, showing a

Table 1 The sheet resistance of different samples

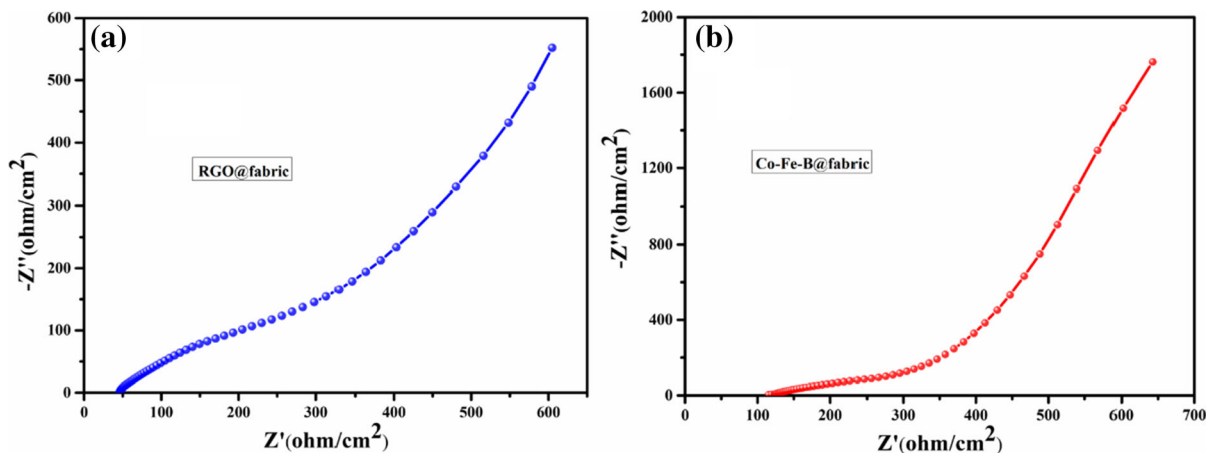| Sample	RGO@fabric	Co2–Fe1–B@RGO @fabric	Co2–Fe1–B@fabric
Sheet resistance	201 Ω/sq	142 Ω/sq	–
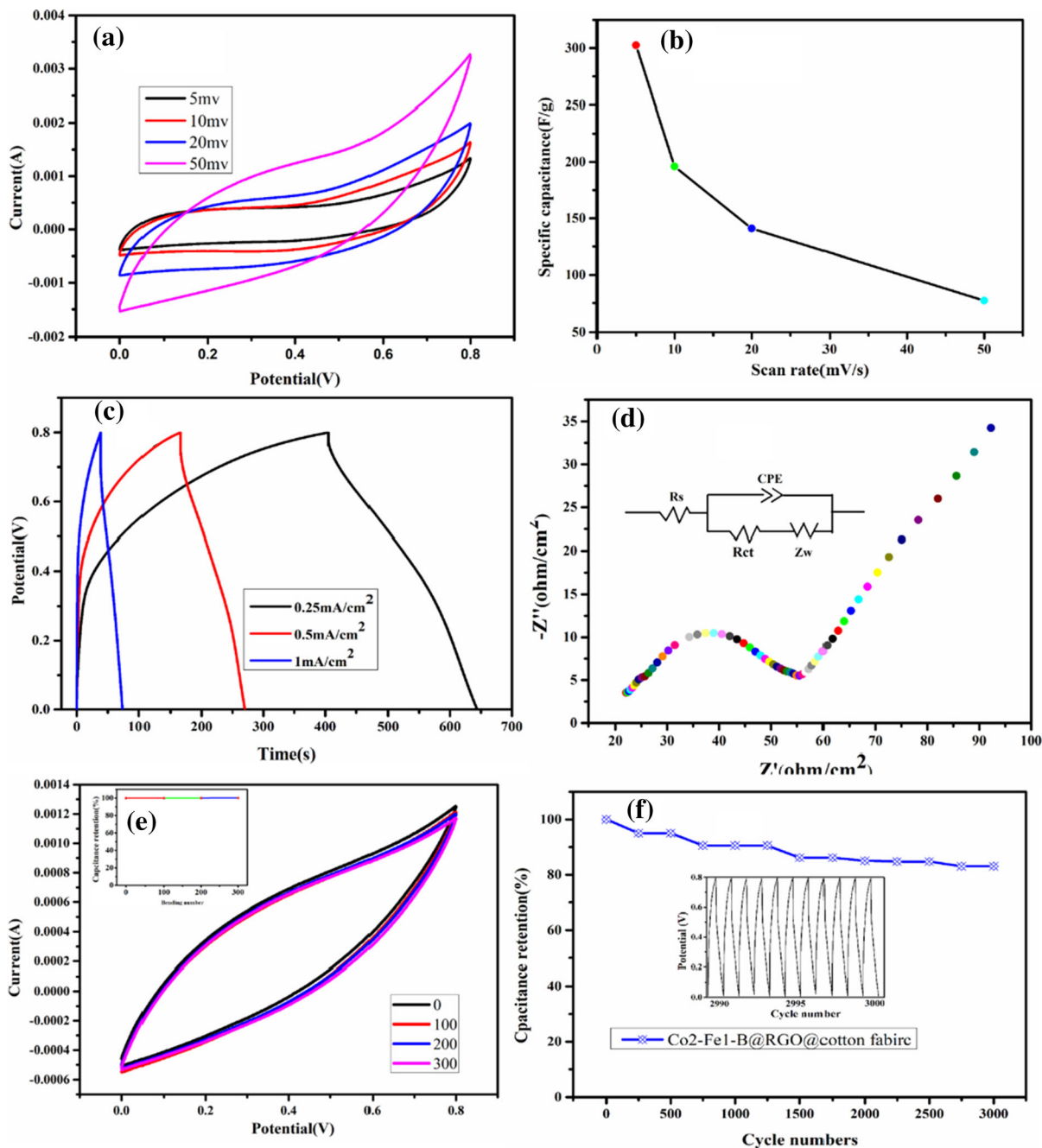
Fig. 9 The capacity of Co2–Fe1–B@RGO@fabric electrode. **a** CV curves at different scan rates; **b** specific capacitance values calculated from CV curves with different scan rate; **c** GCD curves at different current densities; **d** Electrochemical impedance spectroscopy; **e** flexibility test; **f** Cycle life test

splendid electrode conductivity, while Rct is about 37.58 Ω, indicating a fast charge transfer during the electrochemical reaction. The 45° Warburg region exhibited a short projected length in the medium-

frequency, meaning a short ion-diffusion. In low frequency region, Co2–Fe1–B@RGO@fabric exhibited the vertical line, showing the good capacitive behavior (Wan et al. 2017). To further explain the best

Fig. 10 Electrochemical impedance spectroscopy of RGO@fabric and Co2–Fe1–B@fabric

ion transport ability of Co2–Fe1–B@RGO@fabric electrode, EIS results of RGO@fabric and Co2–Fe1–B@fabric were also provided, as shown in Fig. 10. Rs and Rct of Co2–Fe1–B@fabric composite electrode were 115.8 Ω and 170.4 Ω, while those of RGO@fabric composite electrode were 42.8Ω and 262.5Ω. Clearly, Co2–Fe1–B@RGO@fabric has the smallest Rs (20.02Ω) value and Rct (37.58Ω), meaning the highest electrode conductivity and fastest charge transfer. In low frequency region, Co2–Fe1–B@RGO@fabric also exhibited the most vertical line, showing the optimum capacitive behavior. This result mentioned above demonstrated that Co2–Fe1–B@RGO@fabric flexible electrode was of the best electronic transport ability among these three samples.

The flexibility of Co2–Fe1–B@RGO@fabric electrode was studied through bending tests, and the result is presented in Fig. 9e. It was significant that the composite fabric electrode was of excellent bending properties due to overlapped CV curves at different bending cycles. Even being bended for 300 times, CV curve of the electrode was basically identical with that before being bended, suggesting a superior excellent flexibility performance of this electrode.

GCD measurement was also adopted to study the electrochemical stability of as-fabricated Co–Fe–B B alloy@RGO@fabric electrode, and the results are observed in Fig. 9f. The test was performed for 3000 cycles in 1 mol/L of Na_2SO_4 solution at a current density of 1 mA/cm^2, which demonstrated excellent cycling stability. After 3000 cycles, the capacitance

retention of Co2–Fe1–B@RGO@fabric electrode was over 85%.

Conclusion

In summary, amorphous Co–Fe–B alloy@RGO@fabric flexible electrode was firstly designed through simple dipping-drying method combined with chemical reduction at room temperature. Compared with RGO@fabric and Co–Fe–B alloy@fabric electrode, amorphous Co–Fe–B alloy@RGO@fabric electrode showed a maximum specific capacity of 302.6F/g when the scan rate was 5 mV/s. The enhanced capacity of this electrode was mainly due to synergistic effect of high conductivity, more accessible electroactive sites, and rapid electron collection efficiency. This amorphous Co–Fe–B alloy@RGO@fabric electrode also showed excellent flexibility because it could be bent for 300 times without obvious loss of capacitive performance. Based on the results mentioned above, this novel flexible electrode has a promising application in wearable energy storage device.

References

Akanksha J, Vikrant S, Gurmeet S, Sharma RK (2019) Performance enhancement of a supercapacitor negative electrode based on loofah sponge derived oxygen rich carbon through encapsulation of MoO_3 nanoflowers. Sustain Energy Fuels 3:1248–1257. https://doi.org/10.1039/C8SE00562A

Allison L, Hoxie S, Andrew TL (2017) Towards seamlessly integrated textile electronics: methods to coat fabrics and fibers with conducting polymers for electronic applications. Chem Commun 53:7182–7193. https://doi.org/10.1039/C7CC02592K

Chee WK, Lim HN, Zainal Z, Huang NM, Harrison I, Andou Y (2016) Flexible graphene-based supercapacitors: a review. J Phys Chem C 120:4153–4172. https://doi.org/10.1021/acs.jpcc.5b10187

Chen L, Ai Q, Li DP, Si PC, Feng JK, Zhang L, Li YH, Lou J, Ci LJ (2018) Flexible all-solid-state supercapacitors based on freestanding, binder-free carbon nanofibers@polypyrrole@graphene film. Chem Eng J 334:184–190. https://doi.org/10.1016/j.cej.2017.10.038

Chen RN, Liu L, Zhou JS, Hou L, Gao FM (2017) High-performance nickel-cobalt-boron material for an asymmetric supercapacitor with an ultrahigh energy density. J Power Sources 341:75–82. https://doi.org/10.1016/j.jpowsour.2016.11.108

Dong L, Xu C, Li Y, Pan Z, Liang G, Zhou E, Kang F, Yang QH (2016) Breathable and wearable energy storage based on highly flexible paper electrodes. Adv Mater 28:9313–9319. https://doi.org/10.1002/adma.201602541

Feng LX, Wang K, Zhang X, Sun XZ, Li C, Ge XB, Ma YW (2018) Flexible solid-state supercapacitors with enhanced performance from hierarchically graphene nanocomposite electrodes and ionic liquid incorporated gel polymer electrolyte. Adv Funct Mater 28:1704463. https://doi.org/10.1016/j.nanoen.2014.05.022

Heo J, Eom J, Kim YH, Park SK (2018) Recent progress of textile-based wearable electronics: a comprehensive review of materials, devices, and applications. Small 14:1–16. https://doi.org/10.1002/smll.201703034

Hu RF, Zhao J, Zhu GD, Zheng JP (2018) Fabrication of flexible free-standing reduced graphene oxide/polyaniline nanocomposite film for all-solid-state flexible supercapacitor. Electrochim Acta 261:151–159. https://doi.org/10.1021/am404799a

Jeong YK, Son I, Baek SH (2019) Binder-free of NiCo-layered double hydroxides on Ni-coated textile for wearable and flexible supercapacitors. Appl Surf Sci 467–468:963–967

Kowalczyk D, Fortuniak W, Mizerska U, Kaminska I, Makowski T, Brzezinski S, Piorkowska E (2017) Modification of cotton fabric with graphene and reduced graphene oxide using sol-gel method. Cellulose 24:4057–4068. https://doi.org/10.1007/s10570-017-1389-4

Kyu MI, Seonno Y, Jungwoo O (2017) Three-dimensional hierarchically mesoporous $ZnCo_2O_4$ nanowires grown on graphene/sponge foam for high-performance, flexible, all-solid-state supercapacitors. Chem Eur J 3:597–603. https://doi.org/10.1002/chem.201602447

Li X, Tang Y, Song JH, Yang W, Wang MS, Zhu CZ, Zhao WG, Zheng JM, Lin YH (2018a) Self-supporting activated carbon/carbon nanotube/reduced graphene oxide flexible electrode for high performance supercapacitor. Carbon 129(2018):236–244. https://doi.org/10.1016/j.carbon.2017.11.099

Li ZQ, Tian MW, Sun XT, Zhao HT, Zhu SF, Zhang XS (2019b) Flexible all-solid planar fibrous cellulose nonwoven fabric-based supercapacitor via capillarity-assisted graphene/MnO_2 assembly. J Alloy Compd 782:986–994. https://doi.org/10.1016/j.jallcom.2018.12.254

Li Q, Xu YX, Zheng SS, Guo XT, Xue HG, Pang H (2018b) Recent progress in some amorphous materials for supercapacitors. Small 14:1800426. https://doi.org/10.1002/smll.201800426

Li YZ, Zhang YF, Zhang HR, Xing TL, Chen GQ (2019a) A facile approach to prepare a flexible sandwich structured supercapacitor with rGO-coated cotton fabric as electrodes. RSC Adv 9:180–4189. https://doi.org/10.1039/C9RA00171A

Liang AQ, Li DQ, Zhou WQ, Wu YL, Ye G, Wu J, Chang Y, Wang R, Xu JK, Nie GM, Hou J, Du YK (2018) Robust flexible WS_2/PEDOT: PSS film for use in high-performance miniature supercapacitors. J Electroanal Chem 824:136–146. https://doi.org/10.1016/j.jelechem.2018.07.040

Lima MAP, Alcarazespinoza JJ, Silva FAGD, Oliveira HPD (2018) Multifunctional wearable electronic textiles using cotton fibers with polypyrrole and carbon nanotubes. ACS Appl Mater Interface 10:13783–13795. https://doi.org/10.1021/acsami.8b04695

Lin YJ, Gao Y, Fan ZY (2017) Printable fabrication of nano coral-structured electrodes for high-performance flexible and planar supercapacitor with artistic design. Adv Mater 29:1701736. https://doi.org/10.1002/adma.20170173

Liu ZX, Mo FN, Li HF, Zhu MS, Wang ZF, Liang GJ, Zhi CY (2018) Advances in flexible and wearable energy-storage textiles. Small Methods. https://doi.org/10.1002/smtd.201800124

Luo SJ, Zhao JL, Zou JF, He ZL, Xu CW, Liu FW, Huang Y, Dong L, Wang L, Zhang H (2018) Self-standing polypyrrole/black phosphorus laminated film: promising electrode for flexible supercapacitor with enhanced capacitance and cycling stability. ACS Appl Mater Int 10:3538–3548. https://doi.org/10.1021/acsami.7b15458

Meng QZ, Xu W, Zhu SL, Liang YQ, Cui ZD, Yang XJ, Inoue A (2019) Low-cost fabrication of amorphous cobalt-iron-boron nanosheets for high-performance asymmetric supercapacitors. Electrochim Acta 296:198–205. https://doi.org/10.1016/j.electacta.2018.11.067

Nystrom G, Marais A, Karabulut E, Wagberg L, Cui Y, Hamedi M (2015) Self-assembled three-dimensional and compressible interdigitated thin-film supercapacitors and batteries. Nat Commun 6:7259–7259. https://doi.org/10.1038/ncomms8259

Qin W, Liu Y, Liu XY, Yang GW (2018) Facile scalable production of amorphous nickel borate for high performance hybrid supercapacitors. J Mater Chem 40:19689–19695. https://doi.org/10.1039/C8TA07385F

Qiu KW, Yan HL, Zhang DY, Lu Y, Cheng JB, Lu M, Wang CL, Zhang YH, Liu XM, Luo YS (2015) Hierarchical 3D

Co_3O_4@MnO_2 core/shell nanoconch arrays on Ni foam for enhanced electrochemical performance. J Solid State Electr 19:391–401. https://doi.org/10.1007/s10008-014-2611-z

Raula M, Rashi MH, Lai S, Roy M, Mandal TK (2012) Solvent adoptable polymer Ni/NiCo alloy nanochains: highly active and versatile catalysts for various organic reactions in both aqueous and nonaqueous media. ACS Appl Mater Interfaces 4:878–889. https://doi.org/10.1021/am201549a

Sayyed MI, Qashou SI, Khattari ZY (2017) Radiation shielding competence of newly developed TeO_2-WO_3 glasses. J Alloy Compd 696:632–638. https://doi.org/10.1016/j.jallcom.2016.11.160

Senthilkumar V, Kadumudi FB, Ho NT, Kim JW (2016) NiO nanoarrays of a few atoms thickness on 3D nickel network for enhanced pseudocapacitive electrode applications. J Power Sources 303:363–371. https://doi.org/10.1016/j.jposour.2015.11.034

Shen CW, Xie YX, Zhu BQ, Sanghadasa MH, Tang Y, Lin LW (2017) Wearable woven supercapacitor fabrics with high energy density and load-bearing capability. Sci Rep 7:14324. https://doi.org/10.1038/s41598-017-14854-3

Sun C, Li X, Cai ZS, Ge FY (2019) Carbonized cotton fabric in-situ electrodeposition polypyrrole as high-performance flexible electrode for wearable supercapacitor. Electrochim Acta 296:617–626. https://doi.org/10.1016/j.electacta.2018.11.045

Sung JP, Soo WH, Wonryung L, Daishi I, Zhi J, Kilho Y, Hiroaki J, Daisuke H, Masaki S, Tomoyuki Y, Kenjiro F, Keisuke T, Takao S (2018) Self-powered ultra-flexible electronics via nanograting-patterned organic photovoltaics. Nature 561:516–521. https://doi.org/10.1038/s41586-018-0536-x

Tebyetekerwa M, Marriam I, Xu Z, Yang SY, Zhang H, Zabihi F, Jose RJ, Peng SJ, Zhu MF, Ramakrishna S (2019) Critical insight: challenges and requirements of fibre electrodes for wearable electrochemical energy storage. Energy Environ Sci 12:2148–2160. https://doi.org/10.1039/C8EE02607F

Wan C, Jiao Y, Li J (2017) Flexible, highly conductive, and free-standing reduced graphene oxide/polypyrrole/cellulose hybrid papers for supercapacitor electrodes. J Mater Chem A 5:3819–3831. https://doi.org/10.1039/c6ta04844g

Wang S, He P, Xie ZW, Jia LP, He MQ, Zhang XQ, Dong FQ, Liu HH, Zhang Y, Li CX (2019b) Tunable nanocotton-like amorphous ternary Ni-Co-B: a highly efficient catalyst for enhanced oxygen evolution reaction. Electrochim Acta 296:644–652. https://doi.org/10.1016/j.electacta.2018.11.099

Wang Q, Jiao L, Du H, Wang Y, Yuan H (2014b) Fe_3O_4 nanoparticles grown on graphene as advanced electrode materials for supercapacitors. J Power Sources 245:101–106. https://doi.org/10.1016/j.powsour.2013.06.035

Wang YJ, Li XL, Wang YM, Liu Y, Bai Y, Liu R, Yuan GH (2019a) High performance flexible MnO_2@carbonized cotton textile electrodes for enlarged operating potential window symmetrical supercapacitors. Electrochim Acta 299:12–18. https://doi.org/10.1016/j.electacta.2018.12.181

Wang X, Liu B, Liu R, Wang Q, Hou X, Chen D, Wang R, Shen G (2014a) Fiber-based flexible all-solid-state asymmetric supercapacitors for integrated photodetecting system. Angew Chem Int Ed 53:849–1853. https://doi.org/10.1002/anie.201307581

Wang H, Ma Y, Wang R, Key J, Linkovb V, Ji S (2015) Liquid-liquid interface-mediated room-temperature synthesis of amorphous NiCo pompoms fromultrathin nanosheets with high catalytic activity for hydrazine oxidation. Chem Commun 51:3570–3573. https://doi.org/10.1039/C4CC09928A

Wei HH, Huang K, Zhang L, Ge BH, Wang D, Lang JL, Ma JY, Wang D, Zhang S, Li QY, Zhang RY, Hussain N, Lei M, Liu LM, Wu H (2018) Ice melting to release reactants in solution syntheses. Angew Chem Int Ed 57:3354–3359. https://doi.org/10.1002/anie.201711128

Wen P, Fan M, Yang D, Wang Y, Cheng H, Wang J (2016) An asymmetric supercapacitor with ultrahigh energy density based on nickle cobalt sulfide nanocluster anchoring multi-wall carbon nanotubes hybrid. J Power Sources 320:28–36. https://doi.org/10.1016/j.jpowsour.2016.04.066

Xiang CL, Wang QY, Zou YJ, Huang PR, Chu HL, Qiu SJ, Xu F, Sun LX (2017) Simple synthesis of graphene-doped flower-like cobalt-nickel-tungsten-boron oxides with self-oxidation for high-performance supercapacitors. J Mater Chem 5:9907–9916. https://doi.org/10.1039/C7TA00234C

Xing JH, Tao P, Wu ZM, Xing CY, Liao XP, Nie SX (2019) Nanocellulose-graphene composites: a promising nanomaterial for flexible supercapacitors. Carbohyd Polym 207:447–459. https://doi.org/10.1016/j.carbpol.2018.12.010

Xu LL, Guo MX, Liu S, Bian SW (2015a) Graphene/cotton composite fabrics as flexible electrode materials for electrochemical capacitors. RSC Adv 5:25244–25249. https://doi.org/10.1039/C4RA16063K

Xu LS, Jia MY, Li Y, Zhang SF, Jin XJ (2017) Design and synthesis of graphene/activated carbon/polypyrrole flexible supercapacitor electrodes. RSC Adv 7:31342–31351. https://doi.org/10.1039/C7RA04566B

Xu J, Wang D, Yuan Y, Wei W, Duan L, Wang L, Bao H, Xu W (2015b) Polypyrrole/reduced graphene oxide coated fabric electrodes for supercapacitor application. Org Electron 24:153–159. https://doi.org/10.1016/j.orgel.2015.05.037

Yang Y, Li L, Ruan G, Fei H, Xiang C, Fan X, Tour JM (2014) Hydrothermally formed three-dimensional nanoporous $Ni(OH)_2$ thin-film supercapacitors. ACS Nano 8:9622–9628. https://doi.org/10.1021/nn5040197

Zhang YZ, Wang Y, Cheng T, Lai WY, Pang H, Huang W (2015) Flexible supercapacitors based on paper substrates: a new paradigm for low-cost energy storage. Chem Soc Rev 44:5181–5199. https://doi.org/10.1039/C5CS00174A

Zhao J, Li X, Li XY, Cai ZS, Ge FY (2017) A flexible carbon electrode based on traditional cotton woven fabrics with excellent capacitance. J Mater Sci 52:9773–9779. https://doi.org/10.1007/s10853-017-1161-z

Zhou S, Wen M, Wang N, Wu Q, Cheng L (2012) Highly active NiCo alloy hexagonal nanoplates with crystal plane selective dehydrogenation and visible-light photocatalysis. J Mater Chem 22:16858–16864. https://doi.org/10.1039/C2JM32397D